Development of sustainable antibacterial coatings based on electrophoretic deposition of multilayers: gentamicin-loaded chitosan/gelatin/bioactive glass deposition on PEEK/bioactive glass layer

Muhammad Atiq Ur Rehman[1] · Syeda Ammara Batool[1]

Abstract

Developing non-toxic, bioactive, and antibacterial implant devices is an urgent demand in the biomedical field. Here, the antibacterial behaviour and bioactivity of the polyetheretherketone (PEEK)-based coating was enhanced via multi-layer coating approach. This paper presents a study on antibacterial efficiency and in vitro bioactivity of electrophoretically deposited biodegradable gentamicin sulphate (GS)-loaded chitosan (CS)/gelatin (GT)/bioactive glass (BG) layers on PEEK/ BG coatings. As a first layer, PEEK/BG layer was utilized to provide long term stability of the implant and to be a potential reservoir for sustainable drug release. Initially, a Taguchi design of experiment (DoE) approach was adopted to optimize EPD process of CS/GT/BG coatings on 316L stainless steel (316L SS) substrates. Later, CS/GT/BG coatings including GS particles were produced first on the bare 316L SS and then on the PEEK/BG layer. The multi-layered coatings were analysed through morphological, chemical composition, antibacterial activity, drug release capacity, and in vitro bioactivity. The GS was released from the coatings in the controlled manner and minimum inhibitory concentration was maintained even after 3 weeks of incubation. The agar disc diffusion tests confirmed that sustained release of GS provided an antibacterial result against *Escherichia coli* (*E. coli*) *and Staphylococcus carnosus* (*S. carnosus).* Acellular in vitro analysis demonstrated the bioactive nature of the multi-layered coatings by forming an apatite-like layer on the surface of the coatings after 72 h immersion in the simulated body fluid (SBF). Furthermore, the non-toxic behaviour of the multi-layered coatings was confirmed by in vitro cellular studies.

Keywords Electrophoretic deposition · Chitosan · Local drug delivery · Sustainable antibacterial activity

1 Introduction

Biomedical tools reside within millions of individuals and are being implanted in more by new and follow up surgeries every year [1, 2]. As a major component of modern regenerative medicine, their application comprise on hip/ knee replacement, tissue regeneration, prosthesis, and sustained drug release [2, 3]. Metallic implants are commonly used as orthopaedic and internal fixation devices, where the mechanical robustness is needed [2, 4, 5]. The proper fixation and maintaining a stable interface between the host tissue and the implant at both cellular and organ level are of vital importance for orthopaedic joints implantation [6, 7]. The most encountered fixation issues are related with bacterial infection, wear of implant material due to friction, and migration [8, 9]. Due to these problems, osteolysis manifests in the bone bed, causing long-term implant loosening.

Surface coatings can manipulate various insufficiencies in implants by augmenting natural tissue and implant interactions such as bioactivity, resistance to corrosion, localized drug delivery, and cell adhesion [10]. For example, the use of bioactive coatings can enhance the osteoconductivity of metals [11], of which bioactive glasses (BGs) are potential candidates [5, 12, 13]. However, bare bioactive ceramic coatings present some problems such as high coefficient of friction and brittleness, which are generally controlled by

✉ Muhammad Atiq Ur Rehman
atique1.1@hotmail.com

1   Department of Materials Science and Engineering, Institute of Space Technology Islamabad, 1, Islamabad Highway, Islamabad 44000, Pakistan

3886   The International Journal of Advanced Manufacturing Technology (2022) 120:3885–3900

producing composite coatings [14]. The addition of BGs into a biocompatible polymer tailors the coefficient of friction and the elastic modulus of the composite coating in the range of cortical bone [15] [16].

The complexes of biomolecules and/or natural polymers with bioactive ceramics show improved osteointegration and mimic the biological morphologies (biomimetic surfaces) and processes [17]. Therefore, natural polymers have attracted attention owing to their structural similarities with the significant portions of the extracellular matrix (ECM), superior biocompatibility, and biodegradability [18]. A notable polymer found in nature chitosan (CS) presents structural similarity to glycosaminoglycan, a major part in the ECM of bone, which holds a vital role in cell attachment and cell proliferation [18, 19], and thus, it is highly recommended as a coating on the metallic implants [20]. The interface of the coatings with host tissue can be further developed by the introduction of proteins. For example, a polypeptide gelatin (GT), derived from collagen [21], is the main component of the ECM of bone that can be incorporated in the CS-based coatings. The main role of GT is to improve cell attachment, cell differentiation, migration, and proliferation [10]. The tripeptide sequence (RGD sequence) of gelatin facilitates the adhesion of osteoblast cells [22].

Electrophoretic deposition (EPD), being a low cost and versatile technique, can be considered the method of first choice for deposition of novel combinations of biomaterials [23], in which the mobility of charged particles or molecules is harnessed by applying an electric field [24, 25]. In combination to its economic merits, the processing of EPD at ambient temperatures enables the biological macromolecules, cells, and antibacterial drugs to be coated on a conductive substrate or to be infiltrated into a non-conductive materials [23]. CS and its composites can be successfully deposited as a continuous film by EPD with ease. Co-deposition of CS along with GT via EPD was shown to enhance the proliferation of cells and reduction of the cell apoptosis [26]. For example, the introduction of GT in the CS matrix improved shear strength and adhesion to osteoblast-like cells [27]. In vivo and in vitro investigations of chitosan/gelatin (CS/GT) coatings were reported by Keenan [28] which demonstrated the degradation of coatings by lysozymes, accelerating osteogenesis in the early stage of bone healing process. Furthermore, Jiang et al. [27] suggested that the matrix of CS/GT composite might be beneficial for loading functional agents. The focus of research has shifted towards the functionalization of bioactive coatings by assimilating various functional agents, e.g. growth factors, drugs, and enzymes since 2014 [26].

To inhibit the bacterial attachment and formation of biofilm, and to improve the bioavailability of a drug, local drug delivery (DD) systems have taken centre stage in the biomedical applications, recently. Local DD systems assure the required therapeutic amount of a drug over a specified period of time at the site of injury, eliminating the risk of serious infections and speeding up the curing process. Moreover, local DD can decrease the likelihood of toxicity and may impart a persisting bactericidal effect, due to the sustained drug release, which is frequently introduced in a polymer-based matrix [29, 30]. An aminoglycoside antibiotic, gentamicin sulphate (GS), is routinely administered for the nursing of osteomyelitis due to its far-reaching effect against various bacteria [31–33]. GS is frequently incorporated in the coatings to establish a local drug delivery system and to provide long term bactericidal effect [31, 32, 34–38]. Pishbin et al. [39] produced GS-loaded CS/BG coatings that displayed long-lasting antibacterial effect and augmented cell attachment. CaP/CS/GS/carbon nanotube (CNTs) coatings were fabricated on magnesium alloy via EPD by Zhang et al. [40], and the release of GS was controlled by regulating the concentration of CNTs in the composite coating.

In our previous work, we have investigated the in vitro bioactivity and adhesion strength of single polyetheretherketone (PEEK) and BG coatings [41], design of experiment study of single CS/GT/BG coating [42], and osteogenesis and antibacterial activity of multi-layered metallic ions doped-BG/CS/GT on PEEK/BG basal layer [43].

Accordingly, in this research work, we produced multi-layered coatings having sustainable antibacterial activity and non-toxic and bioactive surfaces. The biodegradable top coating (CS/GT stocked with GS by EPD on the biostable bottom layer (PEEK/BG coatings) can be considered an emerging class of multifunctional coatings for metallic implants. Special attention was given to the co-deposition of CS/GT/BG particles at ambient temperature by adopting Taguchi design of experiment (DoE) approach for the optimization of EPD process in economic terms. A detailed microstructural, compositional, and bioactivity analysis is carried out. In order to tackle the increasing issues of bacterial infections related with orthopaedic implants, we doped GS to the top layer and analysed the antibacterial activity and drug release capability of the coatings. The novel classes of multi-layered and multifunctional coatings were designed, produced, and studied, to deploy in the field of EPD coatings for orthopaedic implant applications.

2 Experimental procedure

2.1 EPD

2.1.1 First layer: PEEK/BG coating

We deposited the PEEK/BG bottom layer on a polished 316L SS (medical grade) substrate via EPD, described elsewhere [44]. Briefly, an ethanol-based suspension including 45S5 BG

Springer

particles [45] (4 μm mean particle size, Schott™, Germany), PEEK particles (10 μm average particle size, 704XF Victrex™), and citric acid (VWR™ International) was prepared. A stable and mechanically robust coating of ~80 μm at 15×15 mm^2 area was produced via EPD and sintering. The cleaned 316L SS electrodes were inserted into the suspension facing one another and constant voltage (80 V) was applied for 90 s. The sintering of coatings was done in an air furnace at the temperature of 375 °C for half an hour. PEEK/BG coatings were used as a substrate for the CS/GT layers in the upcoming studies.

2.1.2 Top layer: CS/BG/GT/GS

A clear CS solution was prepared. First, 0.5 g/L of CS (average molecular weight, with 75–85% degree of deacetylation, Sigma Aldrich™) was mixed in 20 vol.% of distilled water and 1 vol.% of acetic acid (VWR international). Then, 79 vol.% of absolute ethanol was included to the CS solution. Separately, a GT solution was formulated. A total of 1.0 g/L GT powder (type B, Fluka™) was mixed in 20 vol.% distilled water and 1 vol.% acetic acid. The mixing was guaranteed by stirring magnetically at the temperature of 45 °C for 60 min. Afterwards, the suspension was gently cooled off under magnetic stirring. Finally, 79 vol.% of ethanol was added to the GT solution after cooling. The individually prepared CS and GT solutions were then mixed in the volume concentration ratio of 50:50. Optimum concentration ratio of CS and GT were determined by using Taguchi design of experiment (DoE) approach (data is not shown here). A total of 0.5 g/L 45S5 BG particles and 2 mg/mL GS (Sigma Aldrich™, Germany) solution in deionized water were poured in the mixed solution. Subsequently, solution was put under magnetic stirring for 5 min and ultrasonicated for 60 min to ensure the uniform dispersion of the solid particles in the solution. The stability of the suspension was confirmed by the zeta-potential measurement with a zetasizer (nano ZS equipment, Malvern Instruments™, UK). BG incorporated CS/GT films were first deposited on the 316L SS substrate to optimize the deposition parameters of EPD process and then the PEEK/BG layer was deposited in the next step. The PEEK/BG-coated 316L SS was used as the substrate and bare 316L SS foils were utilized as the counter electrode for DC-EPD. The distance of 10 mm was kept between electrodes and deposition voltages of 30–50 V were applied for 5 min.

2.2 Characterization of the coatings

2.2.1 Morphological, compositional, and surface roughness analysis

The surface topography and elemental composition of the coatings were characterized by microscopic techniques including field emission scanning electron microscopy (FESEM, LEO 435VP, Carl Zeiss™ AG) and the energy-dispersive x-ray spectroscopy (EDX), respectively. Fourier transform infrared spectroscopy (FTIR) (Nicolet 6700, Thermo Scientific™) was used for chemical compositional analysis of the coatings in transmittance mode ranging from wavenumber of 4000 to 400 cm^{-1}. The crystallographic examination was carried out by X-ray diffraction (XRD) (D8 Advance, Bruker™) in the 2ϑ range of 20 to 80°.

Laser profilometer (UBM, ISC-2) was used to analyse the average and maximum surface roughness of the coatings. In order to measure the surface roughness of the coatings 5–7-mm long line was drawn on the surface of each sample (scanning velocity of 400 points per second).

2.2.2 Drug release capability and antibacterial activity

The amount of GS incorporated in the coatings was quantified by scraping off the substrate and immersed in 1 mL deionized water (borate buffer pH 10.4). After 10 min sonication, the immersion samples were centrifuged and the supernatant was tested for dissolved GS, according to [39]. To quantify the drug release of GS, the multilayer coatings (15×15 mm^2) were immersed in the solution of 10 ml of PBS, and then incubated at the temperature of 37 °C for 60 min upto 21 days (experiment was done in triplicate). At specified time intervals, 2-ml aliquots were extracted and replaced with fresh PBS solution to preserve the physiological conditions. At the wavelength of 248 nm, characteristic absorption peak of GS was measured and monitored by using UV/VIS Spectrometer (Specord40 by Analytikjena) and WinASPECT 2.5.8.0 software, respectively. The percentage of cumulative drug release at each time point (ρ_x) was computed as per Eq. 1, where m_x and m_t represent mass of released drug at individual time intervals and cumulative release of GS in the duration of 180 days, respectively. ρ_x is the percentage of cumulative drug release at each time interval.

$$\rho_x = \frac{m_x}{m_t} \times 100 \tag{1}$$

Agar disc diffusion testing was performed on PBS (control sample), CS/GT/BG, controls, and on the GS-loaded CS/GT/BG coatings (CS/GT/BG/GS). The 10-μL aliquots, which were taken for drug release, were dropped to the paper discs (diameter = 10 mm). Agar culture plates were filled homogeneously with 20 mL of agar and then pouring over it 20 μL of LB-media containing Gram negative bacteria; *Escherichia coli* (*E. coli*) and Gram positive; *Staphylococcus carnosus* (*S. carnosus*) having optical density of 0.015 (OD$_{600}$). The agar plates containing paper discs were then incubated at 37 °C for 24 h. After 24 h, the cultured agar

plates were photographed and images were analysed using 'ImageJ' software for inhibition zones measurement (each test was carried out in triplicate).

2.2.3 In vitro bioactivity studies

SBF tests For in vitro acellular bioactivity evaluation, the coatings were immersed in simulated body fluid (SBF), as suggested by Kokubo and Takadama [46]. Coated samples of 15 mm × 15 mm dimensions were soaked in 50 mL of SBF and then kept in the incubator at the temperature of 37 °C for a duration of 1, 3, 7, and 14 days. Samples were removed from SBF at each specified time interval, rinsed gently with distilled water, and then stored in a desiccator after drying in air. The acellular bioactivity of the coatings was assessed for the formation of apatite like crystals through SEM–EDX, XRD, and FTIR techniques.

Cell studies For in vitro cytocompatibility testing of the coatings, human osteosarcoma cell line MG-63 (commercially available and purchased from Sigma Aldrich, Germany) was used. Disc-shaped multi-layered CS/GT/BG coatings and the coatings of CS/GT/BG/GS on PEEK/BG (having diameter of 13.6 mm) were used for cell studies. PEEK/BG layer and tissue culture plate were used as control samples. Dulbecco's modified Eagle medium (DMEM) was used for cell culture, augmented with 10 vol.% of foetal bovine serum (FBS; Sigma-Aldrich) and 1 vol.% of penicillin/streptomycin (Pen-Strep; Sigma-Aldrich). The arrangement was then placed in the incubator under a humidified atmosphere containing 5% CO_2 (Glaxy 170R, New Brunswick) at 37 °C. To achieve up to 80–90% of confluence, 75 cm^2 canted-neck cell culture flasks (Greiner-Bio One) were used for cell growth for 48 h. The grown cells were then washed with phosphate buffer saline (PBS; Gibco) and used medium was discarded. Afterwards, trypsin/EDTA (Life Technology) was deployed to detach cells from the wall of the flask. The numbers of living cells were counted in a haemocytometer by introducing trypan blue dye (Sigma-Aldrich). The samples containing cells were sterilized in 24-well plate under UV light for 1 h. After sterilization, 1 mL of cell suspension including 10^5 cells/mL was added to each well. The cells were then allowed to grow on the control samples and coatings for 48 h at 5% CO_2 humidity level and 37 °C temperature. For cell viability quantification, the WST-8 (water-soluble tetrazolium salt) test was performed. At each time interval, the used culture medium was removed and replaced with 400 μL fresh DMEM solution containing 1% WST-8 reagent in each well pursued by incubation, following standard protocols (Cell counting kit 8: Sigma Aldrich). A microplate-reader (Anthos-Phomo, Germany) was used to measure absorbance at 450 nm. The absorbance value of the tissue culture plate (positive control)

was taken as 100% cell viability. The viability of the sample coatings was normalized against the positive control. The results obtained from experiments (performed in pentaplicate) were stated as the mean value ± standard deviation (SD). Moreover, for statistical analysis, one-way analysis of variance (ANOVA) with $p < 0.05$, $p < 0.01$, and $p < 0.001$ was adopted and for post hoc analysis, Tukey's range test was utilized (the analysis was carried out using a statistical software; MINITAB 16™).

For qualitative evaluation of the morphology and viability of the cells attached to the coatings surface after 48 h of incubation, the cells were dyed with DAPI (4′,6-diamidino-2-phenylindole) and Calcein^{AM} (Life Technologies, USA). Cells were washed with PBS briefly and then 4 μL Calcein^{AM}/DAPI per mL of PBS was added to the cells. After 60 min of incubation time, samples were again washed with PBS and fixed with a 3.7 wt.% paraformaldehyde (PFA Sigma-Aldrich, Germany) solution. Fluorescence microscopy (FM) (Axio Scope A.1, Carl Zeiss Microimaging GmbH) was used to record cell viability.

SEM analysis was performed to study the cell morphology attached to the multi-layered CS/GT/BG/GS on PEEK/BG layers. To fix the cells to the coatings surface, two different fixing solutions were utilized. SEM-Fixer I solution had the composition of 1 mL of 50% of glutaraldehyde solution (0.1%), 25 g of sucrose, 10 g of paraformaldehyde, and 500 mL of sodium cacodylate trihydrate whereas the composition of SEM-Fixer II solution was 3 mL of 50% glutaraldehyde solution (0.3%), 15 g of paraformaldehyde, and 500 mL of sodium cacodylate trihydrate. At first step, samples were soaked in 1 mL of SEM-Fixer I solution for 45 min and then washed with 1 mL of PBS. At second step, samples were soaked in 1 mL of SEM Fixer II solution for again 45 min and subsequently washed with 1 mL of PBS. Then samples were dehydrated with an increasing ethanol series (purity level 30–99%). In the end, samples were dried supercritically for approximately 60–90 min using EM CPD300 dryer (Leica, Germany).

3 Results and discussion

3.1 Bare chitosan/gelatin/BG coatings

3.1.1 Suspension stability

The stability of the solutions, which depends on intermolecular interactions, was measured by assessing their pH dependent zeta-potential. The pure GT (1.0 g/L) and CS (0.5 g/L) solutions exhibited positive zeta-potentials at pH value of 4.5, which closely agrees with the data found in literature [47]. The mixtures of CS and GT solution also showed a positive zeta-potential calculated as $+45 \pm 7$ mV, at a pH value of 4.5, which was also reported by Ma et al. The

reason for higher zeta potential values could be the repulsive intermolecular interaction between CS and GT, which facilitated the stability of suspension [48]. At acidic pH, CS and GT were charged positively exerting repulsive forces (F_R) among them. However, opposite charge was established on some side groups, due to which they may interact overcoming electrostatic repulsive forces (F_R) [26, 49]. The electrostatic attractions (F_A) between the NH_3^+ groups of CS and COO^- groups of GT may lead towards the formation of a polyelectrolyte complex [50]. As a consequence, although the possible interaction between the CS and GT molecules, no precipitation was occurred, and the clear blend solution had high enough stability for electrophoretic deposition.

The positive zeta-potential value of $+35 \pm 7$ was maintained at the pH value of 4.5 on addition of BG to the CS/GT suspension. The attractive forces between oppositely charged particles, i.e. BG (positive) and side groups of CS/GT (negative), should cause the adsorption of CS/GT molecules on the surface of BG particles at an acidic pH [18], which could facilitate the electro-steric stabilization of the BG particles. Moreover, the hydrophilic groups present in GT were adsorbed on the BG surface. The adsorption of CS/GT molecules on BG surface and positively charged polyelectrolyte were responsible for achieving co-deposition of CS/GT/BG. Therefore, CS/GT polyelectrolyte complex and the BG particles possessing positive zeta-potential migrate towards the cathode under the applied electric field and get deposited on the cathode surface as a continuous film of CS/GT reinforced with BG particles [50].

3.1.2 Statistical analysis

To optimize the working parameters for EPD and composition of the suspension, the Taguchi design of experiment (DoE) approach was applied. It helped achieve high deposition rate and low standard deviation values for the CS/GT/BG coatings (data not presented here). The parameters were optimized at 30 V of the deposition voltage, 5 min of deposition time, and 50:50 ratio of the volume concentrations. The assessment of the kinetics of the EPD process was based on Hamaker's model at the optimum concentration ratio. Figure 1 shows the variation in current density as a function of deposition time at different applied voltages and the deposition yield. The values of current density remained almost constant during the whole deposition time at each applied voltage, i.e. 20 V, 30 V, and 50 V (Fig. 1A). The deposition rate increased with the increase in deposition time and voltage, as expected. However, deposition yield deviated from linearity at the lowest applied voltage and deposition time (10 V; 1 min) and at the highest applied voltage and deposition time (50 V; 9 min). The deposition rate was linear in the range of 20–30 V (Fig. 1B). It may be suggested that the lower applied voltage and short deposition time caused to form an insufficient coating, whereas, the highest voltage (50 V) led to deposit extreme amount of BG particles that would inhibit the deposition of CS and GT matrix. As a result, according to the Taguchi DoE studies, we chose the optimum parameters as 50:50 CS/GT volume concentration, 30 V and 5 min, respectively. The detail study on the optimization of the composite coating was published in [42].

3.1.3 Coating morphology

Figure 2 illustrates the SEM images of surface and cross section, and EDX elemental mapping of SEM analysis of the CS/GT/BG coatings on 316L SS that were produced with optimized EPD parameters, anticipated by DoE approach. The coatings had reasonably homogenous microstructure consisting of a film like layer considered the CS/GTmatrix and reinforced BG particles that were distributed homogenously within the matrix (Fig. 2A). However, a little amount of microspores was spotted in the coatings, for which the reason could be the occurrence of water electrolysis [43]. The cross section of CS/GT/BG showed a uniform coating (film-like structure) of 4–5 μm thickness (Fig. 2B, C). The thickness of coating noted in this study was in accordance to the literature [30, 47, 49].

Fig. 1 A Plot for the variations in current density with deposition time at different voltages. **B** Plot for the variation in the deposition yield at various EPD parameters. (Reproduced from [42])
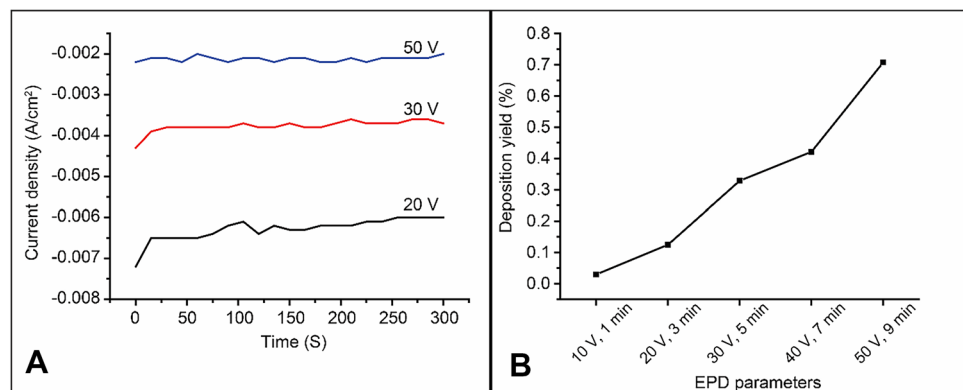
3.2 Multilayer coatings (CS/GT/BG/GS coatings on PEEK/BG layer)

### 3.2.1 Deposition mechanism, morphological, and structural investigations

Deposition phenomenon of multilayer coating Once the optimized parameters for CS/GT/BG coatings deposited over 316L SS were obtained [42], corresponding parameters for EPD and composition of the suspension were used to produce multi-layered coatings by depositing the CS/GT/BG on PEEK/BG layers which were previously attained by EPD. We simply record the value of the current density at 30 V for the deposition time of 5 min with reference to the 316L SS substrate. Upon changing the substrate, i.e. PEEK/BG-coated 316L SS substrate, we apply the 30 V but the value of current density was lower compared to that of the 316L SS substrate. We simply keep on increasing the deposition voltage, i.e. 50 V till the point we achieve the same current density that we obtained for 316L SS substrate at 30 V (the optimum deposition parameter).

The deposition phenomenon of the GS-loaded CS/GT/BG on the PEEK/BG layer is exhibited in Fig. 3. It was reported in the Sect. 2.1 that the suspension including CS and GT molecules and BG particles was charged positively. Therefore, a continuous film of GS-loaded CS/GT/BG was deposited on the cathode surface; in this case, PEEK/BG coated 316L SS. It is worth mentioning that the porosities found in the layer of PEEK/BG may be held responsible for providing a conductive passage to the charged molecules. Furthermore, PEEK/BG coatings were charged negatively at the pH value of 4.5 [44], which may have favoured the deposition of positively charged CS and GT molecules present in the suspension. Therefore, this attractive sort of interaction

between two layers, i.e. PEEK/BG and CS/GT/BG/GS may improve adhesion.

Bottom PEEK/BG layer Figure 4A, B demonstrate the SEM images of surface and cross section of PEEK/BG coatings deposited electrophoretically and then sintered at 375 °C. The surface of the coatings presented a fairly homogenously microstructure including PEEK matrix reinforced with BG particles (Fig. 4A). Moreover, the matrix and the particles were highly packed and uniform thickness of 80–85 μm was achieved. The PEEK/BG-coated 316L SS samples were mechanically robust and would ensure the long-term stability, thus were utilized as the substrates to fabricate multi-layered coatings. The porous nature and rough surface of the coatings is visible from both surface and cross section SEM images. The porosities and valleys in/on the coatings were used as the reservoirs for the top CS/GT-based coatings and were beneficial to the sustainable drug release. The details of the effects of deposition kinetics and sintering on the mechanical properties (adhesion and bending strength) of the coatings was recently published [41].

Morphology of the multilayer coatings Figure 4D, E show the SEM images of the surface and cross section of multilayered coatings. The CS/GT/BG coating penetrated the pores in the PEEK/BG layer to some extent, as displayed in the SEM image of the surface (Fig. 4D). Nevertheless, multilayered coatings maintained the rough surface due to the thin layer of CS/GT/BG/GS and represented the surface of PEEK/BG layer. A thinner, film like layer can be seen on the PEEK/BG layer (Fig. 4E) revealing that CS/GT/BG had lower thickness than that produced on bare 316L SS. The similar protocol was employed by [51] to examine cross-section of the coatings. This result can be considered due to the deposition of the top layer on the rough surface and
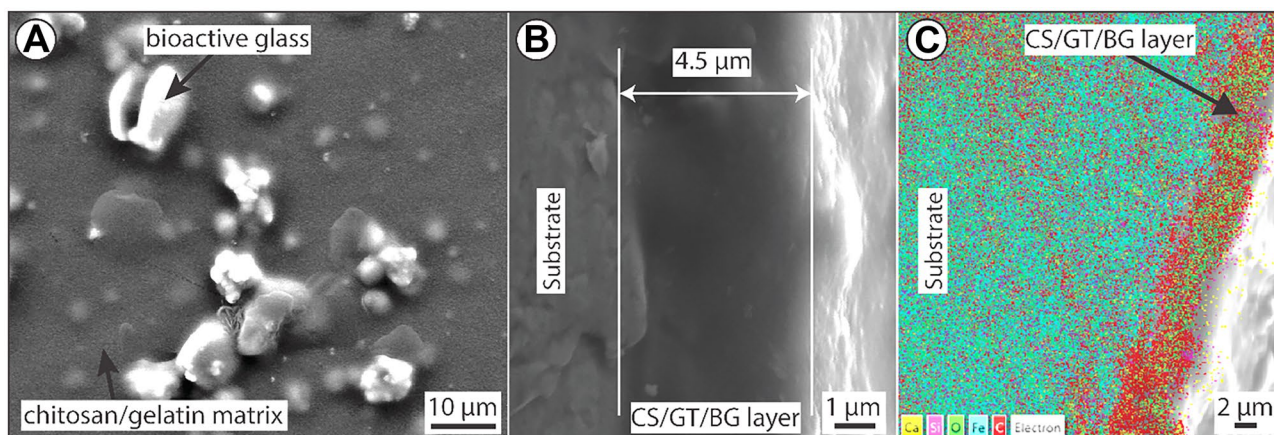
Fig. 2 SEM images of CS/GT/BG (0.5 g/L) coatings on 316L SS produced at 30 V and 5 min of deposition time: **A** image at the surface, **B** image at the cross section, **C** EDX mapping at the cross section. (Reproduced from [42])
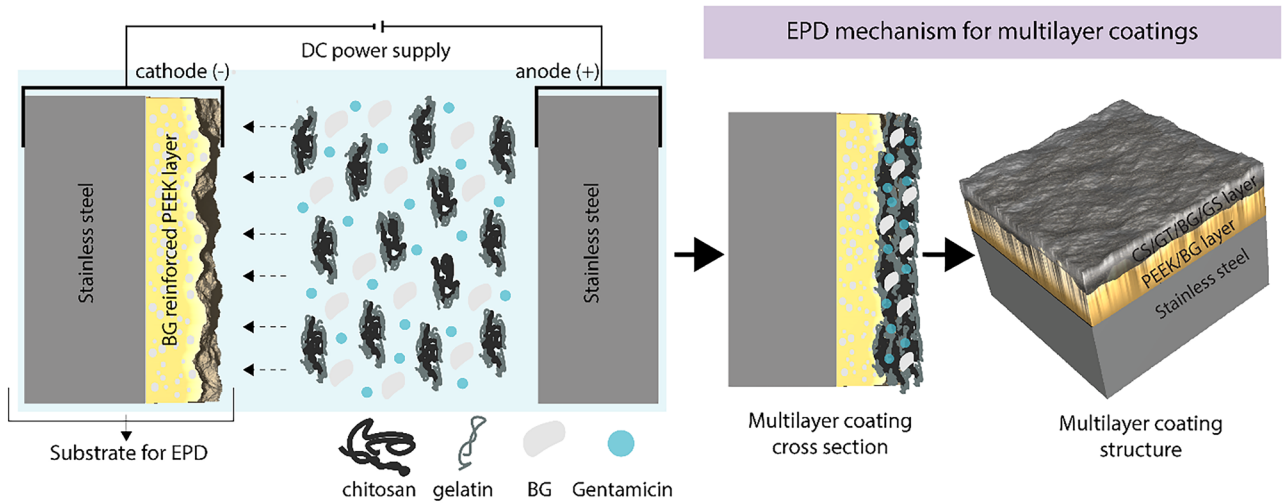
Fig. 3 Schematic illustration of the deposition phenomenon for multi-layer coatings

in the porous structure of the PEEK/BG layer. The conductive pathway made by the porosities at the PEEK/BG layer allows to deposit the CS/GT/BG/GS deep inside the pores of the PEEK/BG layer, which may facilitate the sustained release of the GS over prolonged periods. Figure 4F displayed the presence of GS nanoscale precipitates in the CS/

Fig. 4 SEM images of PEEK/BG and GS-loaded multilayer coatings **A** the surface of coatings of PEEK/BG sintered at 375 °C and **B** the cross section **C** point EDX at BG particles and GS precipitates **D** the surface of GS-loaded CS/GT/BG coatings over PEEK/BG and **E** CS/GT/GS layer cross section, **F** BG particles and GS precipitates displayed at high magnification, **G** elemental distribution across the cross-section of multilayer coatings, and **H** EDX mapping of the multilayer coatings
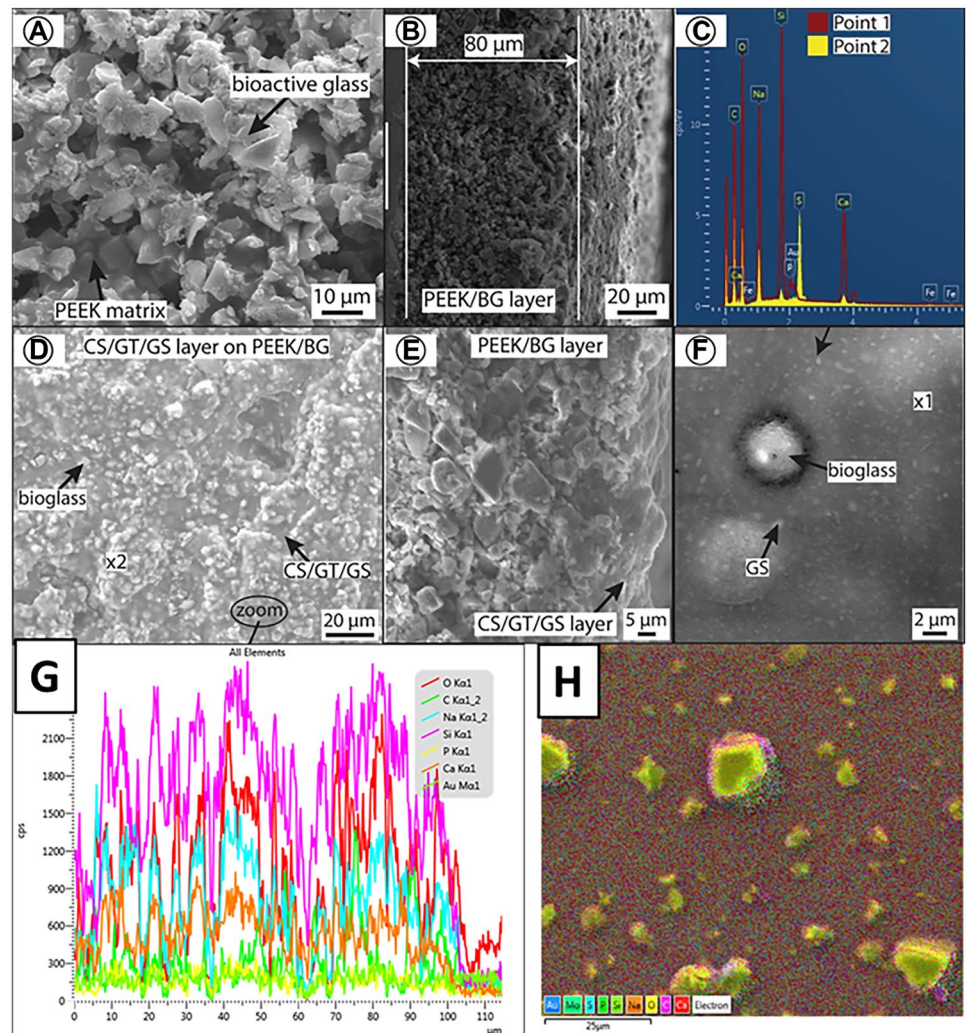
GT/BG coating, and further confirmation of GS precipitates was provided by the EDX analysis, as presented in Fig. 4C. EDX analysis demonstrated the increment in the intensity of sulphur peak of the precipitates and decrement in the intensity of Ca and P peaks, which proved the occupancy of GS in the multilayer coatings qualitatively. Figure 4G shows the elemental distribution across the cross-section of the multilayer coating shown in Fig. 4E. It was observed that the Na, Si, Ca, C, and P are distributed across the cross-section (the presence of Na, Si, Ca, and P is attribute to the BG and the presence of C may indicate the presence of polymeric content in the coatings). Figure 4H shows the elemental EDX mapping of the CS/GT/BG/GS coatings deposited on PEEK/BG layer. It was observed that the BG particles and GS precipitates are dispersed fairly uniform on the top surface of the coatings (S represents GS precipitates whereas Si, Ca, and Na represents BG).

The adhesion strength of the multilayer coatings was not investigated in the current study. However, the adhesion strength of the PEEK/BG layer was studied in our previous studies. PEEK/BG coatings exhibit the adhesion strength of 4B (qualitatively) and 13–18 N qualitatively [2, 3]. The top layer just infiltrated in the porous PEEK/BG layer, therefore, no clear interface was observed. Since the top layer did not show a separate interface. Thus, the adhesion strength of the multilayer coatings is expected to be similar to that of the PEEK/BG coatings (as PEEK/BG layer is in contact with the substrate).

Table 1 shows the elemental composition of CS/GT/BG/GS coatings deposited on PEEK/BG layer. The results of the Table 1 are in agreement with the Fig. 4G, H. It is important to mention that the detection of C via EDX is not accurate. Therefore, the presence of CS/GT and PEEK in the multilayer coatings system was confirmed via FTIR analysis.

Chemical composition of the multilayer coatings The FTIR spectra were taken separately for each set of coatings. For example, first FTIR of PEEK/BG coating was conducted followed by the, CS/GT/BG coating on SS, multilayer coatings and GS-loaded multilayer coatings. The obtained spectrum was plotted in Origin® by using the option "stack lines by offsets". Figure 5 illustrates the FTIR spectra of PEEK/BG,

CS/GT, and multilayered coatings. FTIR bands of PEEK/BG and CS/GT coatings are seen overlapped in the multilayer spectrum. For instance, the FTIR bands of the multilayer coating at 1700 cm^{-1}–1300 cm^{-1} were dominated by the peaks relevant to the polymer that can be referred to the CS, GT, and PEEK molecules. These peaks representing C=O bonds, C-H bonds, and symmetrical stretching of the nitro group were found overlapping at 1651 cm^{-1} [47, 52], 1536 cm^{-1} [53], and at 1454 cm^{-1} [54], respectively. The peaks related to BG particles in the multilayer spectrum were perceived at lower wavenumbers such as phosphate and Si–O–Si bending were spotted at 461 cm^{-1} and 562 cm^{-1}, respectively [44]. The deposition of CS and GT in the multilayer coatings was indicated by the existence of amide I and amide II bands in the multilayer spectrum (Fig. 5). Moreover, the incorporation of GS widens the O–H band as shown in spectrum 4, the reason could be the formation of hydrogen bond between amide groups of CS/GT and O–H group of GS [55]. Even so, FTIR spectra were not able to show convincing proof of the successful deposition of GS in the multilayer coatings.

3.3 Performance analysis of multilayer coatings

3.3.1 Drug release capability

Drug release capability of a device/material is important to investigate whether it can carry or not, a required therapeutic amount of a drug at the targeted site over a certain period of time. Figure 6 shows the curve of drug release obtained for GS for the multilayer coatings. Comparing the fitting of experimental data to four different models, namely the Peppas-Sahlin model was found as the best fitting model

Table 1 Elemental EDX analysis of the GS-loaded CS/GT/BG coatings over PEEK/BG layer

Element	Atomic %
C	73.11
O	20.93
Na	2.05
Si	0.28
S	3.25
Ca	0.37
Total:	100.00
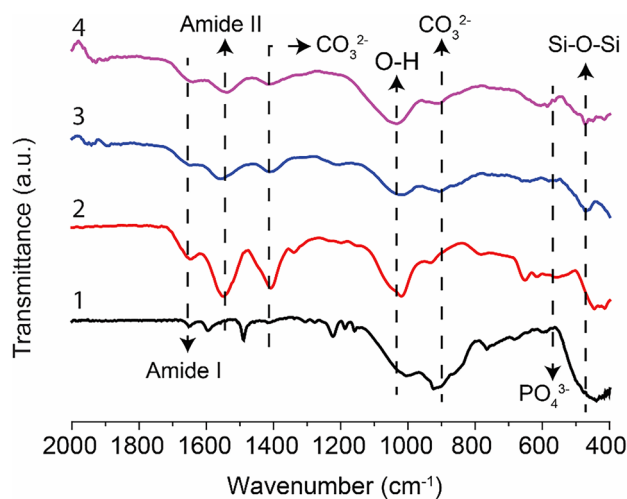
Fig. 5 FTIR spectra of PEEK/BG coating (1), CS/GT/BG coating on SS (2), multilayer coatings (3), and GS-loaded multilayer coatings (4)

with R^2 of 0.9613. The curve presented three main regions. Region-I corresponded to primary burst release of drug at day 1, during which ~ 35% of the drug got liberated mainly due to the direct diffusion of drug from the surface of the multilayer coatings to the PBS (phosphate buffer saline) medium [29, 35, 56]. Therefore, it is right to conclude that on day 1 the drug was mainly released as a result of diffusion mechanism [29, 57]. After 24 h of immersion in PBS medium, the CS/GT film in the upper layer may start degrading [43]. In conclusion, the drug released continuously at accelerated rate, i.e. almost 60% of the drug was released during first 7 days (same effect was reported in the literature [55]). Consequently, it can be hypothesized that after day 1, the combined effect of degradation and diffusion mechanisms governed the kinetics of drug release [58]. As diffusion rate is in direct relation with the concentration gradient, GS released with a higher rate in region-I. In region-II, despite the dissolution of the CS/GT matrix, drug release rate was slowed down by the decreased concentration gradient between the multilayer coating and the medium. In other words, the available dosage of GS in the multilayer coatings reduced after 24 h of incubation period. In the region-III, drug release was very slow due to the fact that degradation of the most of the CS/GT matrix occurred and the little amount of the left over drug in deeper pores of PEEK/BG layer was released at very lower rates in the end. During EPD, the conductive pathway in the porous PEEK/BG coating allows to deposit the GS-loaded top layer into the deeper pores. Therefore, the porous and rough layer of PEEK/BG facilitated the release of GS in a controlled manner over a time period of 21 days, as shown in Fig. 6.

3.3.2 Antibacterial activity

The antibacterial behaviour of multilayer coatings was verified by adopting indirect contact method which showed the generation of inhibition zone on agar medium against bacteria including *S. carnosus* and *E. coli*. The 10-µL aliquots taken from the pristine PBS solution (control), CS/GT/BG coating immersed PBS solution (control) and multilayer coatings immersed PBS solution (sample) were placed on bacteria inoculated plates. The control samples exhibited no antibacterial activity against both bacteria. However, multilayer coatings presented bactericidal effect against *S. carnosus* and *E. coli* (Fig. 7). A bacteria free zone (inhibition zone) was formed around the paper discs. GS, a broad-spectrum antibiotic, released from the multilayer coatings within the immersion time, which was confirmed by the UV/VIS studies, spread to the agar medium, and killed the bacteria to some extent. The molecular structure of GS is responsible for its bactericidal property. GS forms bond with the bacterial cells and produce abnormal proteins having bactericidal effect [37, 55, 59].

To achieve a long-term antibacterial outcome, the drug should be liberated above the minimum inhibition concentration (MIC) in a sustainable manner over longer periods of time. To analyse the antibacterial efficacy, the change in the inhibition halo with the immersion time was calculated using 'ImageJ' software. The largest inhibition zones (halo $= 10 \pm 1$ mm) were exhibited by the multilayer coatings that were incubated in PBS for 6 h. The reason for this result could be the primary burst release and diffusion of the GS from the multilayer coating during the initial 6 h. The

Fig. 6 Cumulative release of GS from the multilayer coatings in PBS (data provided is the mean ± standard deviation for experiments performed in triplicate)
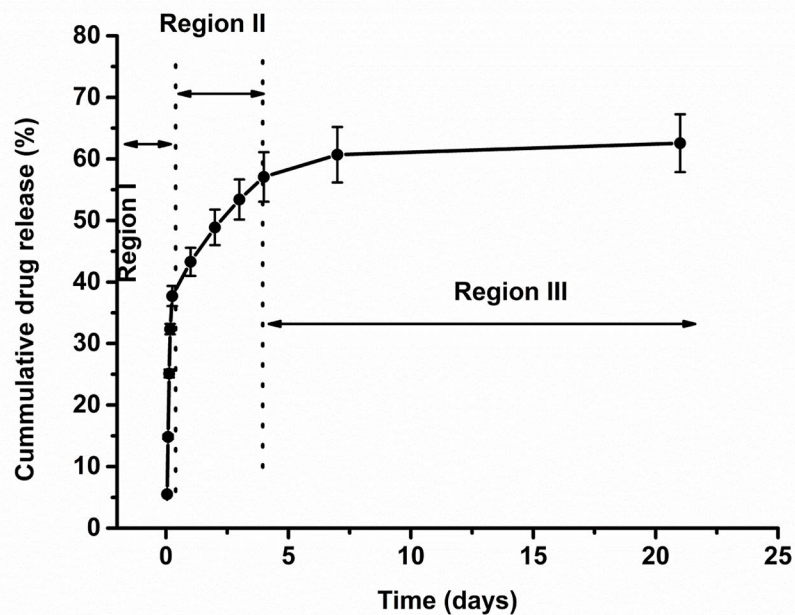
inhibition zone narrowed with increasing incubation time (Fig. 7), which was in accordance to the kinetics of drug release showing the decreased release of the GS due to the degrading of the multilayer coating. However, the released concentration of GS was higher than the minimum inhibitory level (0.2–0.5 mg/L) even after 21 days, which was able to perform antibacterial activity against gram positive and gram negative bacteria [60]. Multilayer coatings were anticipated to present antibacterial effect for longer period of time.

Due to the higher surface roughness and porous structure of the PEEEK/BG, the design of multilayer coating controlled the release of GS; as a result, a zone of inhibition developed even after 2 weeks by the multilayer coatings. The average surface roughness (R_a) measured for the multilayered coating was ~ 1.5 μm. The surface roughness also influences the attachment of bacteria and cells to the coating [61]. With the growing resistance of bacteria towards antibiotics, there is a need to modify the material surface so that it can resist the attachment and spreading of bacterial film. The roughness size achieved is usually comparable with the size of bacteria to effectively inhibit bacterial adhesion to the surface [62]. The fundamental mechanism behind this is the rupture of bacterial cell wall by the sharp grooves on the surface killing the bacteria [63]. Thus, synthesizing modified surface coatings and incorporating antibiotics such as GS in it can provide a potent way out of the bacterial infections. It is concluded that coatings of multilayer structure may be considered a preferred design to control the long term drug release and to maintain prolonged bactericidal affect.

The coatings developed in this study showed the burst release of GS initially. The burst release of GS is useful in preventing the formation of biofilm. The GS release even after 6 h of incubation was enough to develop the zone of inhibition against gram-positive and gram-negative bacteria. On the other hand, the multilayer coating also provided the sustained release of GS. For example, supernatants obtained after 2 weeks of incubation were antibacterial against the both types of bacteria. Thus, we concluded that the multilayer coating developed in this study can provide sustainable antibacterial effect.

3.3.3 In vitro bioactivity

Multilayer coatings (CS/GT/BG/GS coatings on PEEK/BG layers) were soaked in SBF medium for 1, 3, 7, and 14 days, to qualitatively evaluate the bioactivity of coatings. Figure 8 demonstrates the surface SEM images of multilayer coatings soaked in SBF medium up to 14 days. After 1 day of immersion, the surface morphology of the multilayer coatings began changing. A porous layer consisting of nanocrystals was nucleated and grew laterally on the surface (Fig. 8A). The multilayer coatings were completely covered by these nanoparticles after 3 days of incubation, which can be ascribed to the apatite crystals. Moreover, crystals of apatite were observed to grow vertically with increasing immersion time (Fig. 8B). The early formation of crystal of apatite and the subsequent growth of the apatite layer within the immersion time revealed that multilayered coatings were bioactive under in vitro conditions and thus it may be suggested that multilayered coatings would show in vivo osteoconductive property. The good bioactivity of the multilayer coatings may also be attributed to the surface

Fig. 7 Inhibition zone test with gram positive and gram negative bacteria (*E. coli* and *S. carnosus*) for multilayer coatings at different time durations
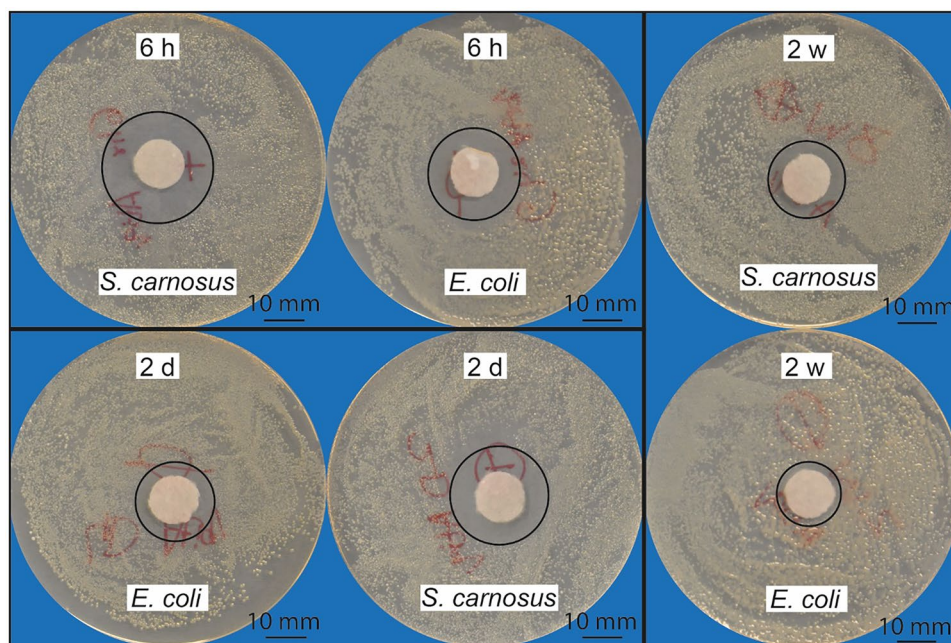
roughness of the coatings [64]. The EDX spectra of the multilayered coatings immersed in SBF for 1 day and 14 days are shown in the inset figures in Fig. 8. The intensity of Si peak (assigned to the BG) decreased after immersion in SBF (Fig. 8A) compared to the EDX pattern before immersion in SBF (Fig. 4C). The decrease in the intensity of the Si peak may indicate the dissolution of BG or the formation of thick apatite-like layer on the surface of coatings. Furthermore, the atomic percent of Ca and P increased with the increase in immersion time (Table 2). The intense and progressive development of the Ca and P peaks with the immersion time implied that the apatite like layer was gradually grown within the immersion time [55, 65].

Figure 9 illustrated the XRD patterns and FTIR spectra of the multilayer coatings immersed in SBF medium for various durations. XRD and FTIR analyses illuminated the carbonated hydroxyapatite formation on the multilayer coatings [66]. New XRD peaks at $2\theta = \sim25.8°$ and at $2\theta = \sim32°$ arisen after 24 h of incubation in SBF medium (Fig. 9A). These peaks can be referred to the formation of hydroxyapatite crystals on the multilayer coatings (the peaks were attributed to HA on the basis of JCPDS-9–432). The intensity of the peaks at $2\theta = 25.8°$ and at $2\theta = 32$ were observed to increase with the time of immersion, indicating the growth of apatite-like crystals [53, 55]. New bands representing phosphate (560 cm^{-1}, 610 cm^{-1}, and 1014 cm^{-1} [67]) and carbonate (873 cm^{-1} and 1400 cm^{-1} [10]) were investigated at the FTIR spectrum of the multilayer coatings immersed in SBF for 1 day (Fig. 9B). Moreover, the intensity of silica peak decreased at increased incubation period. The growth of apatite crystals was confirmed by the relative increase in the intensity of phosphate peaks with the prolonged immersion period [10, 67]. The formation of carbonated hydroxyapatite crystals was confirmed by the presence of carbonate and phosphate bands [68]. Furthermore, FTIR analysis authenticated the bioresorbable character of the CS and GT film at the upper layer. The intensity of the amide-I (1645 cm^{-1} [47]) and amide-II (1558 cm^{-1} and 1406 cm^{-1}

Table 2 Elemental EDX analysis of the multilayer coatings after immersion in SBF for 1 and 14 days

| Element	Atomic % after 1 day of immersion in SBF	Atomic % after 14 days of immersion in SBF
C	19.32	16.83
O	63.59	63.57
Si	0.30	-
Na	1.06	0.47
Mg	0.43	0.42
P	5.86	7.23
Cl	0.70	0.29
Ca	8.50	11.08
Fe	0.25	0.10
Total:	100.00	100.00

[47]) peaks corresponding to relevant bands progressively reduced with the immersion time (Fig. 9B). Therefore, we concluded that CS and GT exhibited the required degradation behaviour upon immersion in SBF medium, which was also in agreement with the data reported in the literature [69].

3.3.4 In vitro cellular studies

Figure 10A, B show the cell density and distribution on PEEK/BG coatings and on tissue culture plate (TCP). It was observed that the cells were uniformly spread on the tissue culture plate with relatively higher cell density in comparison to the PEEK/BG coatings. The relative higher value of average roughness associated with the PEEK/BG coatings led to the decrease in the cell density.

Figure 10C, D demonstrate the cell density and their distribution on the surface of multilayer coatings. Dense and evenly dispersed, living cells in a large number with a relatively large nucleus were spotted on the surface of both coatings (Fig. 10C, D). The images of fluorescence

Fig. 8 SEM images of multilayer coatings after immersion in SBF medium for: **A** 1 day and **B** 14 days (inset figures show the EDX spectra extracted from the surface of the immersed samples)
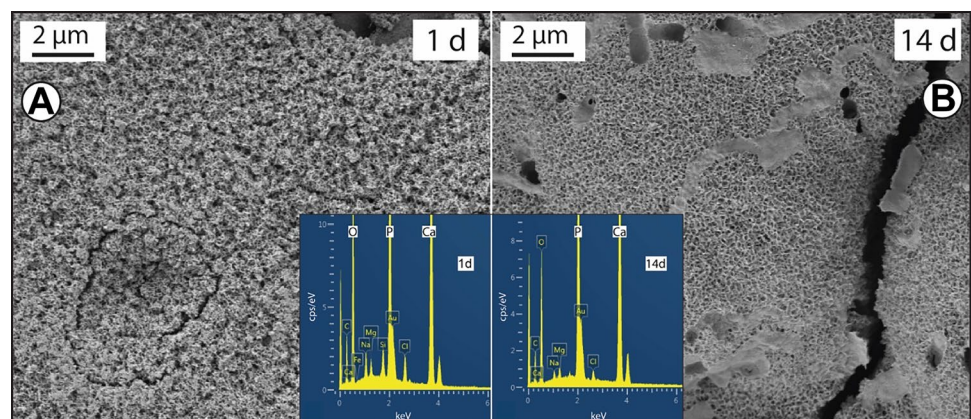
Fig. 9 **A** XRD analysis of multilayer coating before and after immersion in SBF. **B** FTIR analysis of the coatings before and after immersion in SBF
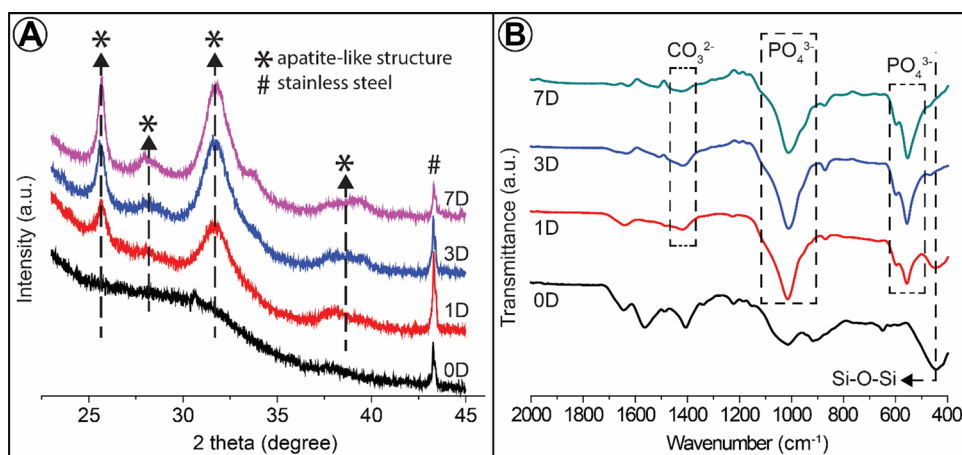

microscopy showed that the GS loading to the multilayer coatings (Fig. 10D) caused no harmful effect on the MG-63 cells growth after 2 days of cultivation as compared to the CS/GT/BG coatings, confirming the biocompatible and non-toxic behaviour of GS in the multilayer coatings. It may be suggested that the hydrophilic nature and rough surface ($R_a \sim 1.5$ µm) of the multilayer coating facilitated the dispersion and attachment of cells, and thus MG-63 cells attached and spread over the surface of coatings [70, 71].

The cellular activity of the CS/GT/BG coatings (with or withoutGS) on the layers of PEEK/BG was investigated by the WST-8 assay based on the percentage of cell viability. Figure 10E displays MG-63 cell viability on the bare PEEK/BG coatings and multi-layered coatings. The coatings of CS/GT/BG and CS/GT/BG/G on PEEK/BG layers facilitated the proliferation of osteoblast-like MG-63 cells in the initial incubation period of 2 days. The differences in cell viability (measured in percentage) between the positive control (tissue culture plate) and the multilayer coatings with and without GS loading were not significant at $p < 0.05$. Furthermore, the percent cell viability was statistically similar for the two multilayer coatings (with and without GS loading), therefore, it can be concluded that the addition of GS caused no cytotoxicity in the multilayer coatings, (Fig. 10E). The results of cell viability studies in relation to the in vitro bioactivity studies (Fig. 9) confirmed loaded multilayer coatings are biocompatibile and bioactive (promote the formation of new bone). Similar results for GS-loaded CS/BG composite coating have been presented by Pishbin et al. [55]. Furthermore, in comparison to the PEEK/BG coating, the incorporation of the top layer (BG reinforced CS/GT layer) enhanced the cell viability, which was in agreement with the literature [72]. We concluded relying on the fluorescence microscopy and cell viability test results that dissolution of BG and the release of GT (and CS) multilayered coatings perseveredsuperior osteoblast cells adherence and proliferation due to the surface topography [21, 70, 71, 73, 74]. Moreover,
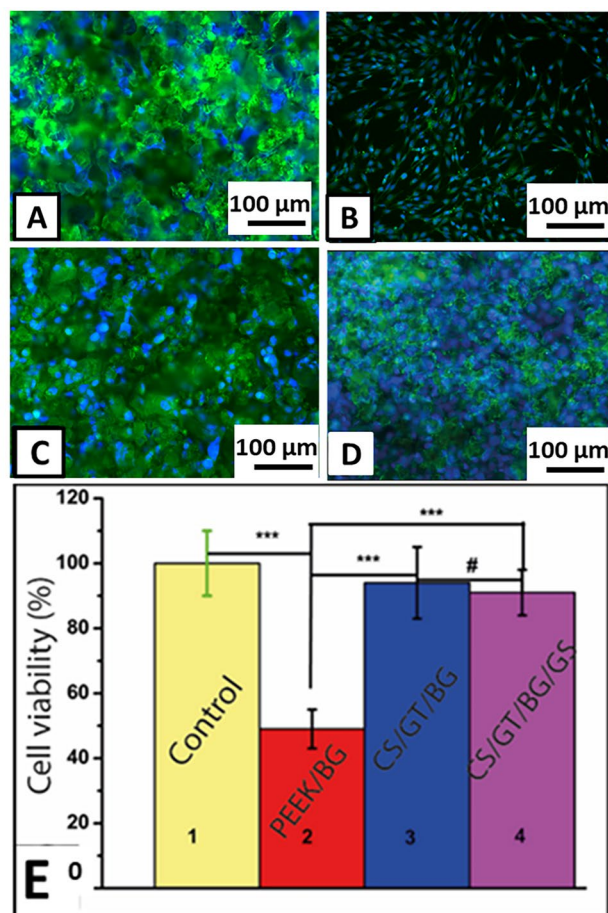
Fig. 10 Fluorescence microscopy images of osteoblast-like MG-63 cells cultured on **A** PEEK/BG coatings, **B** tissue culture plate, **C** GS-loaded multilayer coatings and **D** multilayer coatings stained with Calcein and DAPI after 2 days (live cell in green and nuclei in blue), and **E** osteoblast-like human cells (MG-63) response to (1) tissue culture plate (control), (2) PEEK/BG coatings, (3) multilayer coatings, and (4) GS-loaded multilayer coatings. *** symbolize the significant difference between the two systems at $p < 0.001$ and # symbolize the in-significant difference between the two systems (data presented here is the mean ± standard deviation of two separately performed experiments in pentaplicate)
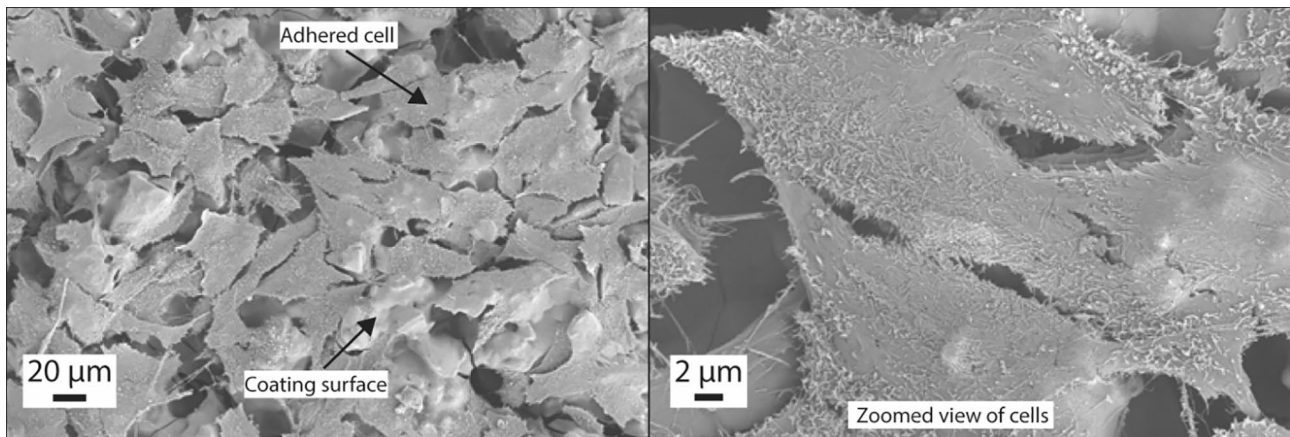
Fig. 11 SEM analysis of MG-63 cells morphology spreading on the surface of CS/GT/BG/GS coatings over PEEK/BG layers incubated for 2 days in cultivation medium

the degradation behaviour is enhanced by the presence of GT, resulting in the reduced steric hindrance and enabling cells to grow and proliferate [72].

The important biochemical behaviour is indicated by the morphology of cells such as adhesion, proliferation, and migration on a relevant material/substrate [75]. Figure 11 conveys the SEM analysis showing morphology of MG-63 cells on the GS-loaded CS/GT/BG on PEEK/BG layer. The SEM images reveal that MG-63 cells got attached on the surface of CS/GT/BG/GS coatings over the provided cultivation period. Due to the presence of high adhesive protein content, the cells got elongated and adopted a strong attachment with the matrix and guided morphology (Fig. 11). The CS/GT matrix degraded with time and the porous and rough surfaced PEEK/BG bottom layer came to the surface causing the embedded cells to experience low steric hindrance [72].

It is concluded by many researches that the peptides responsible for cell binding, specifically RGD sequence helps to improve the osteogenic differentiation of osteoblast cells [61, 76]. The RGD sequence of collagen is incorporated by the GT [77, 78]; we therefore concluded that the RGD peptide found in the coatings stimulates the activity of cell integrin receptors that may play a significant role in osteogenic differentiation. The cell viability and interconnecting cell spreading networks can be enhanced by the presence of GT which confirms the preferability of CS/GT/BG/GS coatings for orthopaedic demands and possibly for bone tissue engineering, e.g. as a coating for scaffolds.

4 Conclusions

In this study, a multi-layered coating was designed to develop a sustainable antibacterial, non-toxic, and bioactive coating. PEEK/BG-deposited 316L SS provided a

potent platform for the deposition of biodegradable CS/GT/BG/GS composite coatings via EPD, in which the working parameters were optimized by Taguchi design of experiment approach (DoE). The final remarks of this research work are listed below:

1. *Compositional and morphological analysis*: The SEM and FTIR analyses indicated the favourable deposition of CS/GT/BG on PEEK/BG layers, whereas EDX and UV/VIS analyses verified the incorporation of GS in the multilayer coatings. The CS/GT/BG/GS coating was uniformly spread on the rough surface of the PEEK/BG layer and penetrated its interconnected porosities to various degrees due to the complicated surface properties owned by the basal PEEK/BG layer. The interconnected porosities, which might create a potential conductive pathway for depositing the top layer to deeper inside the bottom coating, were facilitated as reservoirs for the top layers.

2. *Drug delivery and antibacterial activity*: Multilayer coatings showed GS released in the multi-structure coatings in a sustained way for relatively longer period of time (21 days). As a result, multilayer coatings showed antibacterial effect against both gram-positive and gram-negative bacteria due to the controlled liberation of GS, broad-spectrum antibiotic, to the medium.

3. In vitro *bioactivity and cell studies*: On the surface of multilayer coatings that were immersed in SBF for a short period of time (3 days), a layer similar to apatite was formed indicating the bioactive and osteoconductive nature of the coatings. Furthermore, initial in vitro cellular study clarified that the multilayer coatings, specifically GT, augmented the cell attachment, cell spreading, and cell viability. The non-toxic behaviour of CS/GT/BG/GS coatings was demonstrated by WST-8 assay and

fluorescence microscopy which confirmed the worth of CS/GT/BG/GS coatings for orthopaedic administrations.

The research presented here may lay the foundation for the consideration of multi-structured coatings for in vivo testing and clinical trials.

Declarations

Ethics approval All authors confirm that they follow all ethical guidelines. All authors certify that they have no affiliations with or involvement in any organization or entity with any financial interest or non-financial interest in the subject matter or materials discussed in this manuscript.

Consent to participate The authors agree with the participation.

Consent for publication The authors agree with the publication.

Conflict of interest The authors declare no competing interests.

References

1. Montgomery M, Ahadian S, Davenport Huyer L, Lo Rito M, Civitarese RA, Vanderlaan RD, Wu J, Reis LA, Momen A, Akbari S, Pahnke A, Li RK, Caldarone CA, Radisic M (2017) Flexible shape-memory scaffold for minimally invasive delivery of functional tissues. Nat Mater. https://doi.org/10.1038/nmat4956
2. Barrère F, Mahmood TA, de Groot K, van Blitterswijk CA (2008) Advanced biomaterials for skeletal tissue regeneration: instructive and smart functions. Mater Sci Eng R Reports 59:38–71. https://doi.org/10.1016/j.mser.2007.12.001
3. Kim S (2008) Changes in surgical loads and economic burden of hip and knee replacements in the US: 1997–2004. Arthritis Care Res 59:481–488. https://doi.org/10.1002/art.23525
4. Paital SR, Dahotre NB (2009) Calcium phosphate coatings for bio-implant applications: materials, performance factors, and methodologies. Mater Sci Eng R Reports 66:1–70. https://doi.org/10.1016/j.mser.2009.05.001
5. Hench LL (2005) Repair of skeletal tissues. Biomater Artif Organs Tissue Eng 119–128. https://doi.org/10.1533/9781845690861.3.119
6. Park JB (1992) Orthopedic prosthesis fixation. Ann Biomed Eng 583–594. https://doi.org/10.1007/BF02368607
7. Kitsugi T, Nakamura T, Oka M, Yan WQ, Goto T, Shibuya T, Kokubo T, Miyaji S (1996) Bone bonding behavior of titanium and its alloys when coated with titanium oxide (TiO2) and titanium silicate (Ti5Si3). J Biomed Mater Res 32:149–156. https://doi.org/10.1002/(SICI)1097-4636(199610)32:2%3c149::AID-JBM1%3e3.0.CO;2-T
8. Anthony PP, Gie GA, Howie CR, Ling RS (1990) Localised endosteal bone lysis in relation to the femoral components of cemented total hip arthroplasties. J Bone Joint Surg Br 72:971–979. http://www.ncbi.nlm.nih.gov/pubmed/2246300
9. Geetha M, Singh AK, Asokamani R, Gogia AK (2009) Ti based biomaterials, the ultimate choice for orthopaedic implants - a review. Prog Mater Sci 54:397–425. https://doi.org/10.1016/j.pmatsci.2008.06.004
10. Torkaman R, Darvishi S, Jokar M, Kharaziha M, Karbasi M (2017) Electrochemical and in vitro bioactivity of nanocomposite gelatin-forsterite coatings on AISI 316 L stainless steel. Prog Org Coatings 103:40–47. https://doi.org/10.1016/j.porgcoat.2016.11.029
11. Jones JR (2015) Reprint of: review of bioactive glass: from Hench to hybrids. Acta Biomater 23:S53–S82. https://doi.org/10.1016/j.actbio.2015.07.019
12. Hench LL, Day DE, Höland W, Rheinberger VM (2010) Glass and medicine. Int J Appl Glas Sci 1:104–117. https://doi.org/10.1111/j.2041-1294.2010.00001.x
13. Hench LL, Jones JR (2015) Bioactive glasses: frontiers and challenges, Front. Bioeng. Biotechnol 3:1–12. https://doi.org/10.3389/fbioe.2015.00194
14. Boccaccini AR, Peters C, Roether JA, Eifler D, Misra SK, Minay EJ (2006) Electrophoretic deposition of polyetheretherketone (PEEK) and PEEK/Bioglass® coatings on NiTi shape memory alloy wires. J Mater Sci 41:8152–8159. https://doi.org/10.1007/s10853-006-0556-z
15. Rezwan K, Chen QZ, Blaker JJ, Boccaccini AR (2006) Biodegradable and bioactive porous polymer/inorganic composite scaffolds for bone tissue engineering. Biomaterials 27:3413–3431. https://doi.org/10.1016/j.biomaterials.2006.01.039
16. Baino F, Verne E (2017) Glass-based coatings on biomedical implants: a state-of-the-art review. Biomed Glas 3:1–17. https://doi.org/10.1515/bglass-2017-0001
17. Bellucci D, Sola A, Gentile P, Ciardelli G, Cannillo V (2012) Biomimetic coating on bioactive glass-derived scaffolds mimicking bone tissue. J Biomed Mater Res Part A 100(A):3259–3266. https://doi.org/10.1002/jbm.a.34271
18. Peter M, Binulal NS, Nair SV, Selvamurugan N, Tamura H, Jayakumar R (2010) Novel biodegradable chitosan-gelatin/nano-bioactive glass ceramic composite scaffolds for alveolar bone tissue engineering. Chem Eng J 158:353–361. https://doi.org/10.1016/j.cej.2010.02.003
19. Kumar MNVR (2000) A review of chitin and chitosan applications. React Funct Polym 46:1–27. https://doi.org/10.1016/S1381-5148(00)00038-9
20. Agnihotri SA, Mallikarjuna NN, Aminabhavi TM (2004) Recent advances on chitosan-based micro- and nanoparticles in drug delivery. J Control Release 100:5–28. https://doi.org/10.1016/j.jconrel.2004.08.010
21. Grigore A, Sarker B, Fabry B, Boccaccini AR, Detsch R (2014) Behavior of encapsulated MG-63 cells in RGD and gelatine-modified alginate hydrogels. Tissue Eng Part A 20:2140–2150. https://doi.org/10.1089/ten.tea.2013.0416
22. Chollet C, Chanseau C, Remy M, Guignandon A, Bareille R, Labrugère C, Bordenave L, Durrieu M-C (2009) The effect of RGD density on osteoblast and endothelial cell behavior on RGD-grafted polyethylene terephthalate surfaces. Biomaterials 30:711–720. https://doi.org/10.1016/j.biomaterials.2008.10.033

23. Boccaccini AR, Keim S, Ma R, Li Y, Zhitomirsky I (2010) Electrophoretic deposition of biomaterials. J R Soc Interface 7(Suppl 5):S581–S613. https://doi.org/10.1098/rsif.2010.0156.focus

24. Besra L, Liu M (2007) A review on fundamentals and applications of electrophoretic deposition (EPD). Prog Mater Sci 52:1–61. https://doi.org/10.1016/j.pmatsci.2006.07.001

25. Clifford A, Luo D, Zhitomirsky I (2017) Colloids and surfaces A : physicochemical and engineering aspects colloidal strategies for electrophoretic deposition of organic-inorganic composites for biomedical applications. Colloids Surfaces A Physicochem Eng Asp 516:219–225. https://doi.org/10.1016/j.colsurfa.2016.12.039

26. Patel KD, Singh RK, Lee EJ, Han CM, Won JE, Knowles JC, Kim HW (2014) Tailoring solubility and drug release from electrophoretic deposited chitosan–gelatin films on titanium. https://doi.org/10.1016/j.surfcoat.2013.11.049

27. Jiang T, Zhang Z, Zhou Y, Liu Y, Wang Z, Tong H, Shen X, Wang Y (2010) Surface functionalization of titanium with chitosan/gelatin via electrophoretic deposition: characterization and cell behavior. Biomacromol 11:1254–1260. https://doi.org/10.1021/bm100050d

28. Keenan TR (2012) Gelatin. Polym Sci A Compr Ref 237–247. https://doi.org/10.1016/B978-0-444-53349-4.00265-X

29. Simchi A, Tamjid E, Pishbin F, Boccaccini AR (2011) Recent progress in inorganic and composite coatings with bactericidal capability for orthopaedic applications. Nanomed Nanotechnol Biol Med 7:22–39. https://doi.org/10.1016/j.nano.2010.10.005

30. Cai X, Ma K, Zhou Y, Jiang T, Wang Y (2016) Surface functionalization of titanium with tetracycline loaded chitosan-gelatin nanosphere coatings via EPD: fabrication, characterization and mechanism. RSC Adv 6:7674–7682. https://doi.org/10.1039/C5RA17109A

31. Mouriño V, Boccaccini AR (2010) Bone tissue engineering therapeutics: controlled drug delivery in three-dimensional scaffolds. J R Soc Interface 7:209–227. https://doi.org/10.1098/rsif.2009.0379

32. Zilberman M, Elsner JJ (2008) Antibiotic-eluting medical devices for various applications. J Control Release 130:202–215. https://doi.org/10.1016/j.jconrel.2008.05.020

33. Pilawa B, Ramos P, Krzton A, Liszka B (2012) Free radicals in the thermally sterilized aminoglycoside antibiotics. Pharm Anal Acta 03. https://doi.org/10.4172/2153-2435.1000193

34. Stallmann HP, Faber C, Bronckers AL, Nieuw Amerongen AV, Wuisman PI (2006) In vitro gentamicin release from commercially available calcium-phosphate bone substitutes influence of carrier type on duration of the release profile. BMC Musculoskelet Disord 7:18. https://doi.org/10.1186/1471-2474-7-18

35. Doadrio AL, Sousa EMB, Doadrio JC, Pariente JP, Izquierdo-Barba I, Vallet-Regí M (2004) Mesoporous SBA-15 HPLC evaluation for controlled gentamicin drug delivery. J. Control Release 97:125–132. https://doi.org/10.1016/j.jconrel.2004.03.005

36. Azi ML, Kfuri Junior M, Martinez R, Paccola CAJ (2010) Bone cement and gentamicin in the treatment of bone infection. Background and in vitro study. Acta Ortopédica Bras 18:31–34. https://doi.org/10.1590/S1413-78522010000100006

37. Li XD, Hu YY (2001) The treatment of osteomyelitis with gentamicin-reconstituted bone xenograft-composite. J Bone Joint Surg Br 83:1063–1068. https://doi.org/10.1302/0301-620X.83B7.11271

38. Hetrick EM, Schoenfisch MH (2006) Reducing implant-related infections: active release strategies. Chem Soc Rev 35:780–789. https://doi.org/10.1039/b515219b

39. Pishbin F, Mouriño V, Flor S, Kreppel S, Salih V, Ryan MP, Boccaccini AR, Mourino V, Flor S, Kreppel S, Salih V, Ryan MP, Boccaccini AR, Mouriño V, Flor S, Kreppel S, Salih V, Ryan MP, Boccaccini AR (2014) Electrophoretic deposition of gentamicin-loaded bioactive glass/chitosan composite coatings for orthopaedic implants. ACS Appl Mater Interfaces 6:8796–8806. https://doi.org/10.1021/am5014166

40. Zhang J, Wen Z, Zhao M, Li G, Dai C (2016) Effect of the addition CNTs on performance of CaP/chitosan/coating deposited on magnesium alloy by electrophoretic deposition. Mater Sci Eng C 58:992–1000. https://doi.org/10.1016/j.msec.2015.09.050

41. Rehman MAU, Bastan FE, Nawaz A, Nawaz Q, Wadood A (2020) Electrophoretic deposition of PEEK/bioactive glass composite coatings on stainless steel for orthopedic applications: an optimization for in vitro bioactivity and adhesion strength. Int J Adv Manuf Technol 108:1849–1862. https://doi.org/10.1007/s00170-020-05456-x

42. Atiq M, Rehman U, Azeem M, Schubert DW, Boccaccini AR (2019) Electrophoretic deposition of chitosan / gelatin / bioactive glass composite coatings on 316L stainless steel : a design of experiment study. Surf Coat Technol 358:976–986. https://doi.org/10.1016/j.surfcoat.2018.12.013

43. Nawaz A, Bano SSS, Yasir M, Wadood A, Rehman MAU (2020) Ag and Mn-doped mesoporous bioactive glass nanoparticles incorporated into the chitosan/gelatin coatings deposited on PEEK/bioactive glass layers for favorable osteogenic differentiation and antibacterial activity. Mater Adv 1:1273–1284. https://doi.org/10.1039/D0MA00325E

44. Rehman MAU, Bastan FE, Haider B, Boccaccini AR (2017) Electrophoretic deposition of PEEK/bioactive glass composite coatings for orthopedic implants: a design of experiments (DoE) study. Mater Des 130:223–230. https://doi.org/10.1016/j.matdes.2017.05.045

45. Hench LL (1998) Bioceramics. J Am Ceram Soc 28:1705–1728. https://doi.org/10.1111/j.1151-2916.1998.tb02540.x

46. Kokubo T, Takadama H (2006) How useful is SBF in predicting in vivo bone bioactivity? Biomaterials 27:2907–2915. https://doi.org/10.1016/j.biomaterials.2006.01.017

47. Zhang Z, Cheng X, Yao Y, Luo J, Tang Q, Wu H, Lin S, Han C, Wei Q, Chen L (2016) Electrophoretic deposition of chitosan/gelatin coatings with controlled porous surface topography to enhance initial osteoblast adhesive responses. J Mater Chem B 4:7584–7595. https://doi.org/10.1039/C6TB02122K

48. Gupta AN, Bohidar HB (2007) Surface patch binding induced intermolecular complexation and phase separation in aqueous solutions of similarly charged gelatin - chitosan molecules 10137–10145

49. Cai X, Cai J, Ma K, Huang P, Gong L, Huang D, Jiang T, Wang Y (2016) Fabrication and characterization of Mg-doped chitosan–gelatin nanocompound coatings for titanium surface functionalization. J Biomater Sci Polym Ed 27:954–971. https://doi.org/10.1080/09205063.2016.1170416

50. Voron'ko NG, Derkach SR, Kuchina YA, Sokolan NI (2016) The chitosan-gelatin (bio)polyelectrolyte complexes formation in an acidic medium. Carbohydr Polym 138:265–272. https://doi.org/10.1016/j.carbpol.2015.11.059

51. Motas JG, Gorji NE, Nedelcu D, Brabazon D, Quadrini F (2021) XPS, SEM, DSC and nanoindentation characterization of silver nanoparticle-coated biopolymer pellets. Appl Sci 11. https://doi.org/10.3390/app11167706

52. Rajeswari D, Gopi D, Ramya S, Kavitha L (2014) Investigation of anticorrosive, antibacterial and in vitro biological properties of a sulphonated poly(etheretherketone)/strontium, cerium co-substituted hydroxyapatite composite coating developed on surface treated surgical grade stainless steel for orth. RSC Adv 4:61525–61536. https://doi.org/10.1039/c4ra12207k

53. Pishbin F, Mouriño V, Gilchrist JBB, McComb DWW, Kreppel S, Salih V, Ryan MPP, Boccaccini ARR (2013) Single-step electrochemical deposition of antimicrobial orthopaedic coatings based on a bioactive glass/chitosan/nano-silver composite system. Acta Biomater 9:7469–7479. https://doi.org/10.1016/j.actbio.2013.03.006

54. Wang Y, Guo X, Pan R, Han D, Chen T, Geng Z, Xiong Y, Chen Y (2015) Electrodeposition of chitosan/gelatin/nanosilver: a new

method for constructing biopolymer/nanoparticle composite films with conductivity and antibacterial activity. Mater Sci Eng C 53:222–228. https://doi.org/10.1016/j.msec.2015.04.031

55. Pishbin F, Mouriño V, Flor S, Kreppel S, Salih V, Ryan MP, Boccaccini AR (2014) Electrophoretic deposition of gentamicin-loaded bioactive glass/chitosan composite coatings for orthopaedic implants. ACS Appl Mater Interfaces 6:8796–8806. https://doi.org/10.1021/am5014166

56. Canal C, Pastorino D, Mestres G, Schuler P, Ginebra MP (2013) Relevance of microstructure for the early antibiotic release of fresh and pre-set calcium phosphate cements. Acta Biomater 9:8403–8412. https://doi.org/10.1016/j.actbio.2013.05.016

57. Hixson AW, Crowell JH (1931) Dependence of reaction velocity upon surface and agitation. Ind Eng Chem 23:1160–1168. https://doi.org/10.1021/ie50262a025

58. Kopcha M, Lordi NG, Tojo KJ (1991) Evaluation of release from selected thermosoftening vehicles. J Pharm Pharmacol 43:382–387. https://doi.org/10.1111/j.2042-7158.1991.tb03493.x

59. Hahn FE, Sarre SG (1969) Mechanism of action of gentamicin. J Infect Dis 119(4/5):364–369

60. Andrews JM, Andrews JM (2001) Determination of minimum inhibitory concentrations. J Antimicrob Chemother 48(Suppl 1):5–16. https://doi.org/10.1093/jac/48.suppl_1.5

61. Qu Z, Yan J, Li B, Zhuang J, Huang Y (2010) Improving bone marrow stromal cell attachment on chitosan/hydroxyapatite scaffolds by an immobilized RGD peptide. Biomed Mater 5. https://doi.org/10.1088/1748-6041/5/6/065001

62. Bagherifard S, Hickey DJ, de Luca AC, Malheiro VN, Markaki AE, Guagliano M, Webster TJ (2015) The influence of nanostructured features on bacterial adhesion and bone cell functions on severely shot peened 316L stainless steel. Biomaterials 73:185–197. https://doi.org/10.1016/j.biomaterials.2015.09.019

63. Yoda I, Koseki H, Tomita M, Shida T, Horiuchi H, Sakoda H, Osaki M (2014) Effect of surface roughness of biomaterials on Staphylococcus epidermidis adhesion. BMC Microbiol 14:234. https://doi.org/10.1186/s12866-014-0234-2

64. Zamin H, Yabutsuka T, Takai S, Sakaguchi H (2020) Role of magnesium and the effect of surface roughness on the hydroxyapatite-forming ability of zirconia induced by biomimetic aqueous solution treatment. Mater (Basel, Switzerland). 13:3045. https://doi.org/10.3390/ma13143045

65. Mehdipour M, Afshar A (2012) A study of the electrophoretic deposition of bioactive glass–chitosan composite coating. Ceram Int 38:471–476. https://doi.org/10.1016/j.ceramint.2011.07.029

66. Stoch A, Jastrzębski W, Brożek A, Trybalska B, Cichocińska M, Szarawara E (1999) FTIR monitoring of the growth of the carbonate containing apatite layers from simulated and natural body fluids. J Mol Struct 511:287–294. https://doi.org/10.1016/S0022-2860(99)00170-2

67. Seuss S, Lehmann M, Boccaccini AR (2014) Alternating current electrophoretic deposition of antibacterial bioactive glass-chitosan composite coatings. Int J Mol Sci 15:12231–12242. https://doi.org/10.3390/ijms150712231

68. Kim JH, Kim SH, Kim HK, Akaike T, Kim SC (2002) Synthesis and characterization of hydroxyapatite crystals: a review study on the analytical methods. J Biomed Mater Res 62:600–612. https://doi.org/10.1002/jbm.10280

69. Ma K, Cai X, Zhou Y, Zhang Z, Jiang T, Wang Y (2014) Osteogenetic property of a biodegradable three-dimensional macroporous hydrogel coating on titanium implants fabricated via EPD. Biomed Mater 9:15008. https://doi.org/10.1088/1748-6041/9/1/015008

70. Kim HK, Jang JW, Lee CH (2004) Surface modification of implant materials and its effect on attachment and proliferation of bone cells. J Mater Sci Mater Med 15:825–830. https://doi.org/10.1023/B:JMSM.0000032824.62866.a1

71. Radda'a NS, Goldmann WH, Detsch R, Roether JA, Cordero-Arias L, Virtanen S, Moskalewicz T, Boccaccini AR (2017) Electrophoretic deposition of tetracycline hydrochloride loaded halloysite nanotubes chitosan/bioactive glass composite coatings for orthopedic implants. Surf Coatings Technol 327:146–157. https://doi.org/10.1016/j.surfcoat.2017.07.048

72. Sarker B, Zehnder T, Rath SN, Horch RE, Kneser U, Detsch R, Boccaccini AR (2017) Oxidized alginate-gelatin hydrogel: a favorable matrix for growth and osteogenic differentiation of adipose-derived stem cells in 3D. ACS Biomater Sci Eng 3:1730–1737. https://doi.org/10.1021/acsbiomaterials.7b00188

73. Sarker B, Papageorgiou DG, Silva R, Zehnder T, Gul-E-Noor F, Bertmer M, Kaschta J, Chrissafis K, Detsch R, Boccaccini AR (2014) Fabrication of alginate–gelatin crosslinked hydrogel microcapsules and evaluation of the microstructure and physico-chemical properties. J Mater Chem B 2:1470. https://doi.org/10.1039/c3tb21509a

74. Chen Q, Garcia RP, Munoz J, Pérez De Larraya U, Garmendia N, Yao Q, Boccaccini AR (2015) Cellulose nanocrystals-bioactive glass hybrid coating as bone substitutes by electrophoretic co-deposition: in situ control of mineralization of bioactive glass and enhancement of osteoblastic performance. ACS Appl Mater Interfaces 7:24715–24725. https://doi.org/10.1021/acsami.5b07294

75. Hassan W, Dong Y, Wang W (2013) Encapsulation and 3D culture of human adipose-derived stem cells in an in-situ crosslinked hybrid hydrogel composed of PEG-based hyperbranched copolymer and hyaluronic acid. Stem Cell Res Ther 4:1. https://doi.org/10.1186/scrt182

76. Shin H, Zygourakis K, Farach-Carson MC, Yaszemski MJ, Mikos AG (2004) Modulation of differentiation and mineralization of marrow stromal cells cultured on biomimetic hydrogels modified with Arg-Gly-Asp containing peptides. J Biomed Mater Res 69A:535–543. https://doi.org/10.1002/jbm.a.30027

77. Sarker B, Singh R, Silva R, Roether JA, Kaschta J, Detsch R, Schubert DW, Cicha I, Boccaccini AR (2014) Evaluation of fibroblasts adhesion and proliferation on alginate-gelatin crosslinked hydrogel. PLoS One 9:1–12. https://doi.org/10.1371/journal.pone.0107952

78. Rosellini E, Cristallini C, Barbani N, Vozzi G, Giusti P (2009) Preparation and characterization of alginate/gelatin blend films for cardiac tissue engineering. J Biomed Mater Res - Part A 91:447–453. https://doi.org/10.1002/jbm.a.32216